Aalborg Universitet

AALBORG UNIVERSITY
DENMARK

Modeling Multi-frequency Characteristics for Classroom and Hall Scenarios at 2-4, 9-11 and 27-29 GHz Bands

Zhang, Guojin; Nielsen, Jesper Ødum; Cai, Xuesong; Kentaro , Saito; Hanpinitsak, Panawit ; Takada, Jun-ichi; Pedersen, Gert Frølund; Fan, Wei

Modeling Multi-Frequency Characteristics for Classroom and Hall Scenarios at 2-4, 9-11 and 27-29 GHz Bands

GUOJIN ZHANG[1], **JESPER ØDUM NIELSEN**[1], **XUESONG CAI**[1],
KENTARO SAITO[2], **(Member, IEEE), PANAWIT HANPINITSAK**[2], **(Member, IEEE),**
JUN-ICHI TAKADA[2], **GERT FRØLUND PEDERSEN**[1], **(Member, IEEE),**
AND WEI FAN[1], **(Senior Member, IEEE)**

[1]Antennas, Propagation and Millimetre-Wave Systems Section, Department of Electronic Systems, Faculty of Engineering and Science, Aalborg University, 9220 Aalborg, Denmark
[2]Department of Transdisciplinary Science and Engineering, School of Environment and Society, Tokyo Institute of Technology, Tokyo 1528552, Japan

Corresponding author: Xuesong Cai (xuc@es.aau.dk)

ABSTRACT This paper investigates the wideband channel characteristics obtained in a classroom and a hall indoor scenarios at 2-4, 9-11 and 27-29 GHz. A virtual uniform circular array (UCA) based channel sounding system was utilized to capture wideband spatial channel characteristics. The propagation parameters of multipath components (MPCs) were estimated by using a high resolution parameter estimation (HRPE) algorithm. The estimated MPCs are further grouped into clusters via a novel clustering identification algorithm based on the KPowerMeans algorithm. The comparison of the composite and cluster-level characteristics at multiple frequency bands in both scenarios is investigated. Moreover, the impact of the indoor room environment, i.e. dimension and furniture, on the propagation channel is also analyzed. The statistics of channel parameters at multiple frequency bands extracted constitute a stochastic clustered spatial channel model.

INDEX TERMS Multi-frequency bands propagation, clustering, channel sounding, channel measurement, channel estimation.

I. INTRODUCTION

The centimeter-wave (cm-wave) and millimeter-wave (mm-wave) spectra have been envisioned to support more data traffic and higher system capacity in the fifth generation (5G) communications [1]–[3]. The frequency bands from 450 MHz to 85 GHz are considered as candidates for 5G communications by "Mobile and wireless communications Enablers for the Twenty-twenty Information Society" (METIS) project [4]. Since the channel characteristics at mm-wave frequencies differ from those below 6 GHz [5], it is necessary to establish realistic spatio-temporal channel models at different frequency bands for 5G communication networks.

Extensive research on channel characteristics at different cm-wave and mm-wave frequencies have been done [5]–[8].

The associate editor coordinating the review of this manuscript and approving it for publication was Haruna Chiroma.

It is found that mm-wave transmission suffers significant atmospheric attenuation and cannot penetrate most solid materials very well compared with lower frequency. Besides, reflection is more dominant than diffraction and diffuse scattering at mm-wave bands [7], [9]. Because of these channel characteristics at mm-wave frequencies, 5G communication systems require highly directional antennas, large antenna array, and adaptive beamforming techniques [10]. Understanding the angular characteristics is critical for 5G communications. For this purpose, a considerable amount of measurement-based investigations can be found in the literature, which are mainly divided into two categories: those using a rotated directional antenna (RDA)-based method [9], [11]–[13], [16] or a uniform virtual array (UVA)-based method [16]–[19]. *i)* For the RDA-based method, a highly directional antenna with a certain half-power-beamwidth (HPBW), such as a horn antenna, is rotated to scan the azimuth and elevation directions. The drawback of this

IEEE Access

G. Zhang *et al.*: Modeling Multi-Frequency Characteristics for Classroom and Hall Scenarios at 2-4, 9-11 and 27-29 GHz Bands

method is the spatial resolution limited by the beamwidth of the antenna. In [11], directional horn antennas with 17° HPBW at 25.5 and 28 GHz, 11° HPBW at 37.5 and 39.5 GHz, connected with a time-domain mm-wave channel sounder were utilized to conduct measurement campaigns in a conference room. Frequency-dependent channel parameters with different polarimetric combinations, including root-mean-square (RMS) delay and angular spread, were investigated. Besides, in [9] directional horn antennas with 10° HPBW in both the azimuth and elevation planes were used for the in-building and urban cellular communication systems at 28 GHz. Spatio-temporal channel characteristics and detailed cluster analysis of both the intra- and inter-cluster distributions were investigated. Moreover, in [12] the measurement was conducted at Helsinki Airport in the 15, 28, and 60 GHz bands by means of directional wideband channel sounding using directive horn antennas with 10° and 40° HPBWs in the azimuth and elevation domains, respectively. Channel characteristics at 15, 28, and 60 GHz bands were analyzed and compared by the parameters of the specular propagation paths, specular and diffuse power contributions, polarization, and the delay and angular spreads. In addition, extensive wideband indoor propagation measurements were conducted using rotatable directional horn antennas with 28.8°/30° azimuth/elevation HPBW and 15°/15° azimuth/elevation HPBW, for 28 GHz and 73 GHz, respectively in [13]. Channel characteristics including large-scale path loss models and temporal statistics derived from these measurements were investigated. *ii)* For the UVA-based method, an antenna is moved to different positions with a step less than a half wave-length to form a uniform virtual array, which usually takes a long time to finish one measurement snapshot. In [16], both RDA and UVA methods were adopted and compared to investigate the channel at 60 GHz in a 3D space, including the azimuth and elevation information. In [17], massive multiple-input multiple-output (MIMO) channel measurements at 11, 16, 28, and 38 GHz bands in indoor office environments were conducted by using a vector network analyzer (VNA) and large virtual rectangular arrays. Massive MIMO propagation properties, such as spherical wavefront, cluster birth-death, and non-stationarity over the antenna array were investigated. By applying a virtual uniform cylindrical array in [18], the diffuse scattering of radio waves in 3, 10 and 28 GHz bands were evaluated. It was found that the power and the angular spread of diffuse scattering tend to decrease as the frequency increased. In [19], the authors studied the frequency dependent characteristics at the 5.8, 14.8, and 58.7 GHz bands by a virtual uniform cubic array. However, these works lack the comparison of channel propagation characteristics at multiple frequency bands in different indoor scenarios with the same channel sounding and measurement configuration. Moreover, the impact of the indoor room environment, i.e. dimension and furniture, on channel propagation characteristics has not been fully investigated.

The current work will analyze data measured in the frequency bands of 2-4, 9-11 and 27-29 GHz obtained in a classroom and a hall scenarios using a virtual uniform circular array (UCA) based channel sounding system. The data at 2-4, 9-11 and 27-29 GHz was previously analyzed in [20]–[23] and the data at 27-29 GHz was previously investigated in [24]. In [20], the frequency characteristics of geometry-based clusters at the frequency bands 2-4, 9-11 and 27-29 GHz in the hall scenario were investigated. The cluster intensity and spread characteristics of geometry-based clusters in the classroom scenario at 9-11 and 27-29 GHz, and in both the hall and classroom scenarios at 27-29 GHz were also investigated in [21] and [22], respectively. In [20]–[22], the space-alternating generalized expectation-maximization algorithm (SAGE) was utilized for extracting the parameters of multipath components (MPCs) by assuming the same number of paths for different frequency bands. However, the actual number of MPCs in the frequency bands can be different, due to the channel sparsity at mm-wave frequency bands [25]. Suitable number of paths assuming for each frequency band is necessary to obtain accurate estimation results. Moreover, spatial non-stationarity in realistic channel, such as the power variation across the antenna elements should also be considered [26]. Therefore, to fully and realistically extract the parameters of the MPCs, a complexity-efficient high resolution parameter estimation (HRPE) algorithm is needed. Meanwhile, geometry-based clusters were estimated by the enhanced scattering point-based KPowerMeans (SPKPM) algorithm in [20]–[22] and categorized into different groups based on the propagation mechanism. The results show that specular reflections are not significantly frequency dependent, while shadowing, scattering, diffraction, and the Fresnel zone plate effect had significant frequency dependency. However, [20]–[22] lacks the comparison of channel characteristics in different scenarios at different frequency bands. In [23], the characteristics of path loss and delay-angular profile in the classroom scenario at the frequency bands 2-4, 9-11 and 27-29 GHz were analyzed, where a beamforming method with low angular resolution was exploited. In addition, in [24], four large-scale UCA based measurement campaigns were conducted in various indoor scenarios, including classroom, office, and hall scenarios, at the frequency band 27-29 GHz. The spatial channel characteristics were investigated and compared in the composite level parameters, such as decay factor, delay spread, angular spread and line of sight power ratio. But these works [23], [24] lack the analysis of cluster-level parameters and frequency dependence of these channel parameters.

To address the above-mentioned gaps, we present measurement-based results for indoor measurement campaigns at the frequency bands of 2-4, 9-11 and 27-29 GHz in classroom and hall scenarios. To the best of authors' knowledge, no publication has considered all of these contributions listed as follows:

G. Zhang *et al.*: Modeling Multi-Frequency Characteristics for Classroom and Hall Scenarios at 2-4, 9-11 and 27-29 GHz Bands

IEEE *Access*

- A complexity-efficient high-resolution parameter estimation (HRPE) algorithm [26] is utilized for fully extracting spherical channel propagation parameters of the MPCs with the spatial non-stationarity of path gain considered, resulting in more accurate and realistic estimation. Besides that, based on the HRPE estimation results, composite level parameters, such as path loss, number of paths, RMS delay spreads and azimuth spreads at 2-4, 9-11 and 27-29 GHz frequency bands are investigated.

- A novel cluster identification algorithm based on the automatic KPowerMeans method [28] is proposed to group the estimated MPCs into clusters at multiple frequency bands. The novelty is that we consider both the consistency and difference at different bands. That is, the specular reflections are dominant at multiple frequency bands, and the frequency dependence of specular reflections is not significant [29], [30], which was shown in [20]. Therefore, we utilize the clustering results at mm-wave bands as initialization for lower bands with richer MPCs. This enables us to track the similarities at different bands, identify the additional characteristics at lower bands and compare them realistically. The cluster-level parameters at 2-4, 9-11 and 27-29 GHz frequency bands are statistically modeled, which is essential for performance evaluation for 5G and beyond systems.

- Using the same measurement system in different scenarios and frequency bands, the frequency dependence of channel parameters and the impact of the indoor room environment (i.e. dimension and furniture) are also investigated.

The rest of the paper is organized as follows. Sect. II elaborates the scenarios and specifications in the measurement campaigns. Sect. III presents some typical channels at multiple frequency bands in both scenarios. The HRPE results and composite level parameters are investigated. In Sect. IV, a novel cluster identification algorithm based on KPowerMeans algorithm is introduced. Moreover, cluster-level parameters are elaborated. Finally, conclusions are in Sect. V.

II. MEASUREMENT CAMPAIGN

In this section, two measurement campaigns conducted in classroom and hall scenarios at 2-4, 9-11 and 27-29 GHz frequency bands are introduced. The measurements were performed with a virtual UCA-based VNA channel sounding system, see [23], [24], [31] for more details. A commercial omnidirectional biconical antenna (A-INFO-SZ-2003000/P [32]) is exploited as the transmitter (Tx) antenna and a homemade biconical antenna [33] is used as the receiver (Rx) antenna. The Rx antenna is rotated from the 0th array position clockwise with a pre-set radius $r = 0.24$ m to form $P = 360$ UCA elements. A total of 20 positions were measured for each scenario by moving the Tx. The HPBW in elevation plane of the commercial omnidirectional biconical antenna
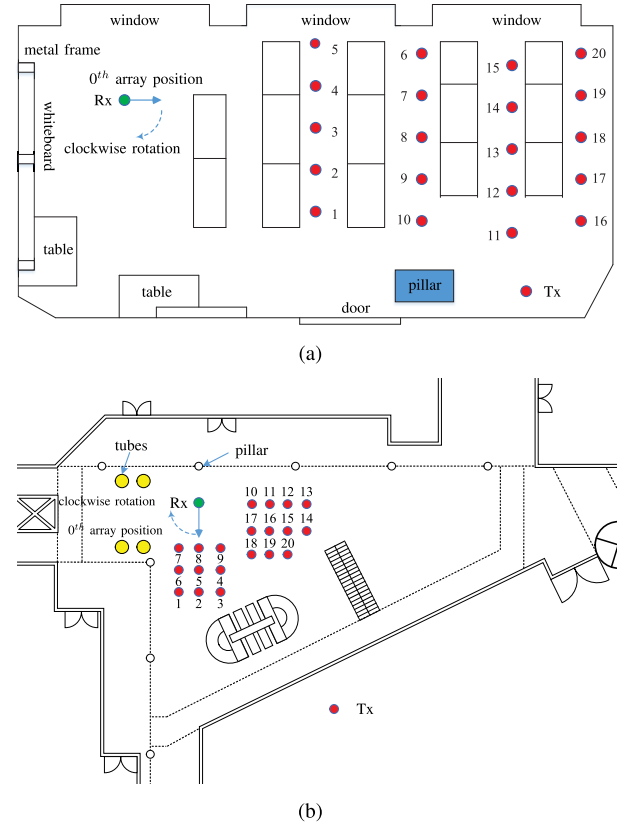
FIGURE 1. The top-view of the classroom and hall where measurement campaigns were conducted. (a) The classroom scenario. (b) The hall scenario.

is less than 30° for 3, 10, and 28 GHz, and the elevation HPBW of the homemade biconical antenna varies from 30° to 65° over the covered band. Due to the narrow beamwidth of the antennas in the elevation plane and typical handset level height [13] for Device-to-device (D2D) connections of 5G communications, the height of both Tx and Rx antennas is set as 1.50 m [34]. Considering the sweep time and the maximum propagation distance for the indoor scenarios, 750 frequency sweeping points were collected for the frequency range 2-4, 9-11 and 27-29 GHz. Table 1 summarizes the measurement specifications.

The first scenario is a classroom with desks and whiteboard as depicted in Fig 1(a), and each Tx location in each row was spaced 0.8 m apart. The dimension of the classroom is $8.54 \times 6.70 \times 2.71$ m^3. The second scenario is a hall with four ventilation tubes and seven white pillars as shown in Fig 1(b). The dimension of the hall is $39 \times 20 \times 10$ m^3, which is much larger than the classroom. In the hall scenario, the Tx grid spacing is 1 m. The details of the measurement scenarios can be found in [24]. Note that, due to the small antenna aperture of the UCA available for the elevation angle information, we only consider the azimuth angle for the angular parameters of the channel in this work. Besides that, it should also be noted that all the measured Tx antenna positions in both classroom and hall scenarios result in LoS scenarios.

IEEE *Access*

G. Zhang *et al.*: Modeling Multi-Frequency Characteristics for Classroom and Hall Scenarios at 2-4, 9-11 and 27-29 GHz Bands

|	
Frequency range	2-4, 9-11 and 27-29 GHz
UCA array radius	0.24 m
Tx/Rx height	1.50 m
UCA elements number	360
Frequency points	750

III. CHANNEL CHARACTERISTICS

A. CONCATENATED CHANNEL IMPULSE RESPONSES

As mentioned above, at each Tx position $P = 360$ UCA elements were collected and 750 frequency points were recorded for each frequency band. The inverse discrete Fourier transform (IDFT) was applied for processing the measured channel transfer functions (CTFs) $H(p, f)$ to obtain the channel impulse responses (CIRs) $h(p, \tau)$, where p is the UCA element index and f is the frequency. To compare the channel characteristics in different scenarios at all bands, we plot the power of 360 CIRs at each Tx position as concatenated CIRs (CCIRs) i.e. $|h(p, \tau)|^2$. Note that the delay resolution is 0.5 ns (corresponding to 0.15 m in distance), due to the 2 GHz bandwidth set for the three frequency bands. Thus, the delay variations of propagation trajectories across the array aperture with radius of 0.24 m can also be observed.

In the classroom Position 5 alongside the window and in the hall scenario Position 5 surrounded by pillars and tubes are chosen as typical positions for the investigation. Figs. 2(a) and 2(b) illustrate the CCIRs for Tx position 5 in the classroom and hall scenarios, respectively, at 2-4, 9-11 and 27-29 GHz. As MPCs rarely have delays larger than 100 ns in both classroom and hall scenarios, it is plotted with a maximum delay of 100 ns to show the details of LoS path and strong reflections more clearly. The noise floor is about -95, -100 and -95 dB for the classroom and hall scenarios at 27-29 GHz, 9-11 GHz and 2-4 GHz, respectively. For fair observation and comparison from Figs. 2(a) and 2(b), the dynamic range 30 dB is set for different frequency bands in both scenarios. We have the following observations shown as below.

- In Figs. 2(a) and 2(b), the shapes of the LoS paths are ")"-alike curves, due to the fact that it is close to the maximum delay and minimum power at the 180th UCA element as well as the minimum delay and maximum power at the 360th or 0th UCA elements at position 5 in both classroom and hall scenarios. That means that the shapes of the paths can reflect the information of the angles-of-arrivals (AoAs). It can be inferred that the LoS paths are approximately from 0 or 360 degree in the azimuth plane. Besides that, another strong reflection path can also be observed after the LoS path in Fig. 2(a). Considering the similar shape of the strong reflection path with LoS path and the delay information, it can be inferred that this path is contributed by the window as indicated in Fig. 1(a).
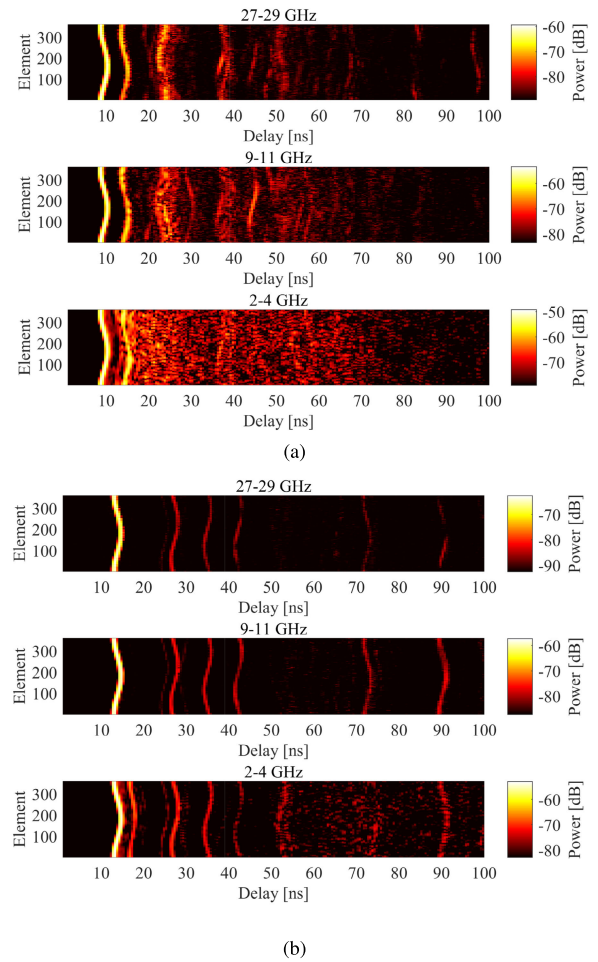
FIGURE 2. The example CCIRs for Tx position 5 in the classroom and hall scenarios at 2-4, 9-11 and 27-29 GHz. (a) Classroom scenario. (b) Hall scenario.

- The MPCs with different shapes can be observed in both Figs. 2(a) and 2(b), which are contributed by other furniture, windows, the sidewalls in the classroom and hall. Different from the "clean" trajectories at 9-11 GHz and 27-29 GHz in both Figs. 2(a) and 2(b), the trajectories may be blurred at 2-4 GHz. It can also be observed that the trajectories of the MPCs are rather sparse at 27-29 GHz in both Figs. 2(a) and 2(b), while much richer at 2-4 GHz. This phenomenon matches the condition known as channel sparsity in [25] that the number of significant MPCs associated with the mm-wave band may be lower than that in sub-6 GHz frequency bands.

- By comparing Fig. 2(a) and Fig. 2(b) at the same frequency bands, it is found that the CCIRs in Fig. 2(a) are much richer than that in Fig. 2(b). We conjecture that it is mostly due to the larger dimension and less furniture of the hall scenario. Besides that, there are more high order reflections and more scattering effects from furniture and sidewalls in the small classroom.

G. Zhang *et al.*: Modeling Multi-Frequency Characteristics for Classroom and Hall Scenarios at 2-4, 9-11 and 27-29 GHz Bands

IEEE *Access*

The above observations demonstrate that the propagation parameters (e.g. delays and azimuths) of MPCs can be roughly obtained by the CCIRs. However, due to the interference among the paths caused by the effect of the IDFT sidelobes and the shapes of different trajectories shifting with respect to the AoAs, the trajectories of the MPCs are blurred in CCIR figures. Therefore, a HRPE algorithm is applied in this paper for estimating high-resolution information of the channel.

B. PARAMETER ESTIMATION

To establish an accurate and realistic channel model, comprehensive and complexity-efficient HRPE algorithms are required for extracting the spherical propagation parameters in ultra-wideband large-scale arrays for future communications. Furthermore, the realistic spatial non-stationarity in path gain across the array elements should be considered as well [26]. Therefore, based on the ultra-wideband and spherical wave propagation model assumption, the HRPE algorithm [26] is exploited to fully extract the spherical channel propagation parameters, i.e. delays, azimuths, elevations, complex amplitudes of the MPCs from the measured CTFs $H(p, f)$. As mentioned above, the UCA radius r was set as 0.24 m. Due to the large aperture, the spherical propagation model must be assumed to avoid the model mismatch that may occur with the plane wave assumption [27]. With a finite number of L spherical waves assumed to impinge on the UCA, the underlying signal model for the measured CTFs $H(p, f)$ contributed by all the L paths can be formulated as [26]

$$H(p, f) = \sum_{\ell=1}^{L} \frac{d_\ell}{d_{p,\ell}} \alpha_\ell e^{-j2\pi f\left(\frac{d_{p,\ell}-d_\ell}{c}+\tau_\ell\right)} + n(p, f) \qquad (1)$$

with

$$d_{p,\ell} = \sqrt{d_\ell{}^2 + r^2 - 2rd_\ell \sin\theta_\ell \cos(\phi_\ell - \phi_p)} \qquad (2)$$

where f is frequency points, α_ℓ, τ_ℓ, θ_ℓ and ϕ_ℓ represent the complex amplitude, propagation delay, elevation and azimuth of the ℓth path, d_ℓ is the distance between the UCA center and the last source point during the propagation, $d_{p,\ell}$ denotes the distance from the pth UCA element to the last source point, c is the light speed, ϕ_p is the azimuth of the pth UCA element calculated as $\frac{2\pi(p-1)}{P}$ and $n(p, f)$ denotes the complex Gaussian noise.

The HRPE algorithm[1] [26] mainly includes three parts. *i)* Firstly, the high resolution estimation results of delays and amplitudes at each element are obtained based on the SAGE principle. In this step, the number of paths should be set large enough to fully extract all the propagation paths at individual antenna elements above the noise floor. *ii)* Secondly, a single path trajectory is identified by the phase mode excitation

technique roughly with the delay and angular information [35]. *iii)* Thirdly, reconstruct the CTFs for this identified path from the second step and update the estimated parameters based on the maximum likelihood principle. Then, update the trajectories by removing this identified path. Go through this ''identification-removing'' operation by repeating steps *ii)* and *iii)*, until the channel power is adequately extracted within the dynamic range. Moreover, the number L of the MPCs can be automatically estimated.
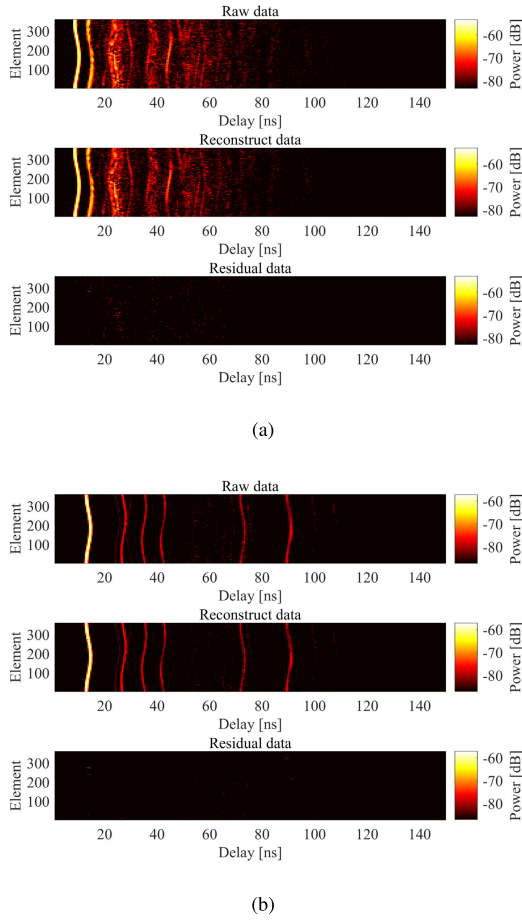
In [26], it is validated that the computation complexity is decreased significantly compared to the maximum likelihood estimator (MLE) algorithm [27] with exhaustive 4D parameter searchings. Considering that a trajectory may be spatially non-stationary across the array elements, a trajectory with a low number of array elements will not be extracted as a valid path. In this way, a complexity-efficient algorithm and more realistic results will be achieved by avoiding the artificial paths with the stationary gain being estimated. The final extracted number of paths L is illustrated in Table 2. To show that the HRPE algorithm has the ability to fully extract the propagation trajectories, we compare the CCIRs of raw data and reconstructed data based on the HRPE estimation results, and residual data obtained by subtracting the reconstructed data from the raw data for Tx position 5 in the classroom and hall scenarios in Fig. 3. It is observed that reconstructed CCIRs are close to raw CCIRs in both Fig. 3(a) and Fig. 3(b). It is found that on average, about 95.5% of total measured power can be extracted for all Tx positions in both scenarios at all bands.

Figs. 4 and 5 illustrate the example estimated power-delay-azimuth spectrums (PDAS) at position 5 for both classroom and hall scenarios in all frequency bands. By comparing Figs. 4 and 5, we have the observations as follows: *i)* The estimated number of paths L is least in Fig. 5(a) and most in Fig. 4(c), which is consistent with the observation from CCIRs in Fig. 2. *ii)* In both Figs. 4 and 5, the azimuths of LoS paths are close to 360° or 0°, which also matches the observation in Fig. 2. *iii)* Using the delays, azimuths of the MPCs and the geometry of the scenarios, it can be inferred that the strong reflections in Fig. 4 are contributed by the metal frame of the whiteboard and window, while the reflections in Fig. 5 are from the pillars and yellow ventilation tubes. *iv)* The delays and azimuths of the LoS path and the strong MPCs are almost the same at different frequencies in the same scenarios in Figs. 4 and 5, respectively. In this way, the weak MPCs around these strong MPCs with similar delays and angles can be considered as clusters.

C. COMPOSITE LEVEL PARAMETERS

Based on the estimated propagation parameters of the channel, composite-level parameters that include the number of paths, path loss, composite root-mean-square (RMS) delay spreads and composite RMS azimuth spreads are investigated.

---

[1]The reader is referred to [26] for details of the extraction of spherical channel propagation parameters using the HRPE algorithm.

IEEE *Access*

G. Zhang *et al.*: Modeling Multi-Frequency Characteristics for Classroom and Hall Scenarios at 2-4, 9-11 and 27-29 GHz Bands

FIGURE 3. The CCIRs of raw data, reconstructed data based on the HRPE estimation results and residual data, respectively, for Tx position 5 in the hall and classroom scenario at 9-11 GHz. (a) Classroom scenario. (b) Hall scenario.

TABLE 2. Statistics extracted for the composite-level parameter.

	Parameters	Classroom	Hall
27-29 GHz	$\text{PL}^{\text{CI}}(n, \varsigma)$	(2.17, 1.06)	(2.81, 1.41)
	$\text{PL}^{\text{FI}}(\alpha, \beta, \varsigma)$	(65.63, 1.52, 0.51)	(68.47, 1.69, 0.83)
	$L\,(\mu, \sigma)$	(64.25, 18.83)	(26.75, 12.41)
	$\sigma_\tau\,[\text{ns}]\,(\mu, \sigma)$	(11.53, 1.77)	(14.89, 31.92)
	$\sigma_\phi\,[^\circ]\,(\mu, \sigma)$	(50.30, 70.01)	(24.79, 56.92)
9-11 GHz	$\text{PL}^{\text{CI}}(n, \varsigma)$	(1.67, 0.61)	(1.97, 0.60)
	$\text{PL}^{\text{FI}}(\alpha, \beta, \varsigma)$	(53.95, 1.44, 0.51)	(53.71, 1.77, 0.56)
	$L\,(\mu, \sigma)$	(100.60, 56.88)	(60, 138.42)
	$\sigma_\tau\,[\text{ns}]\,(\mu, \sigma)$	(14.30, 3.99)	(16.55, 27.81)
	$\sigma_\phi\,[^\circ]\,(\mu, \sigma)$	(50.91, 84.17)	(26.48, 70.77)
2-4 GHz	$\text{PL}^{\text{CI}}(n, \varsigma)$	(1.77, 0.90)	(2.17, 0.70)
	$\text{PL}^{\text{FI}}(\alpha, \beta, \varsigma)$	(45.67, 1.20, 0.41)	(44.90, 1.71, 0.52)
	$L\,(\mu, \sigma)$	(140.65, 15.08)	(104.45, 298.89)
	$\sigma_\tau\,[\text{ns}]\,(\mu, \sigma)$	(17.03, 2.00)	(22.00, 33.80)
	$\sigma_\phi\,[^\circ]\,(\mu, \sigma)$	(54.53, 128.22)	(30.99, 99.45)

1) PATH LOSS PL

The path loss for each location in both the classroom and hall scenarios can be calculated as follows

$$\text{PL} = P_{T_X} - P_{R_X} + G_{T_X} + G_{R_X}$$
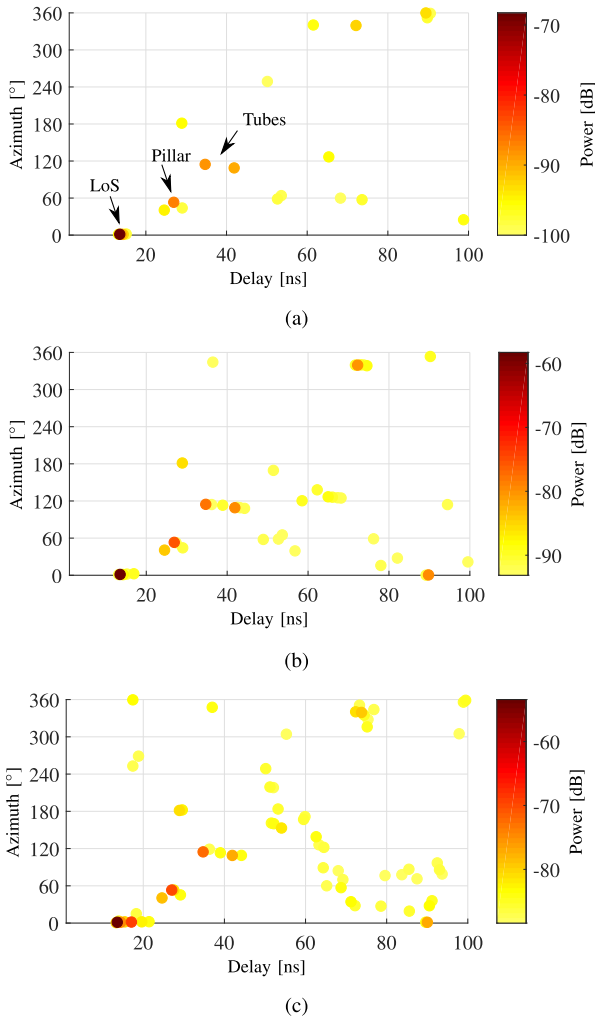$$= -\sum_{\ell=1}^{L} |\alpha_\ell|^2 + G_{T_X} + G_{R_X} \qquad (3)$$
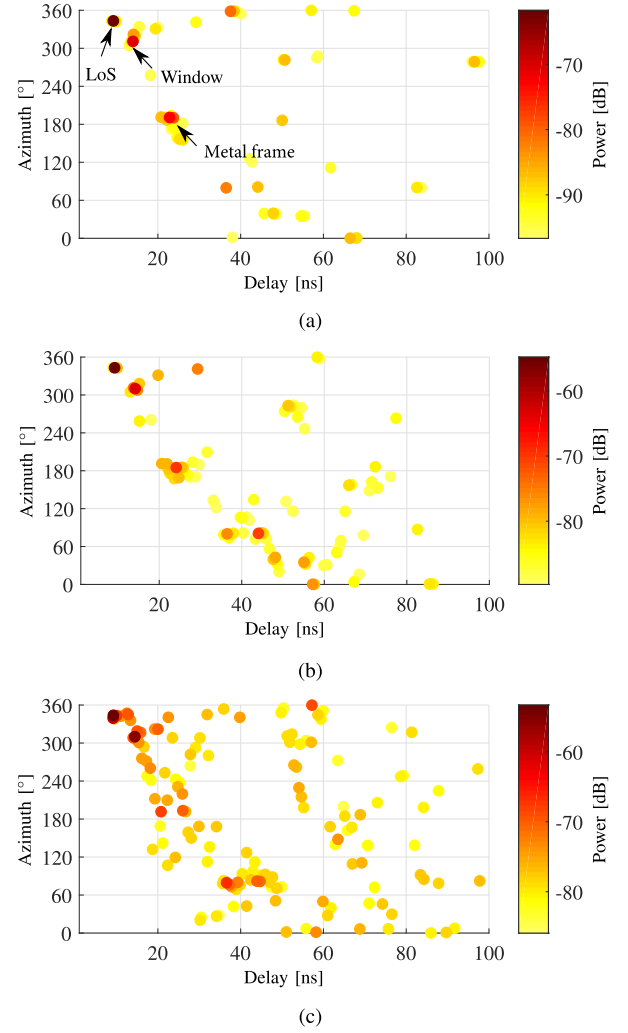
FIGURE 4. The example estimated PDASs for Tx position 5 in the classroom scenario at multiple frequency bands. (a) 27-29 GHz. (b) 9-11 GHz. (C) 2-4 GHz.

where P_{T_X} and P_{R_X} are the transmit power and received power, respectively. In addition, G_{T_X} and G_{R_X} are the gains of the Tx and Rx antennas used at the measured frequency, respectively. The gains of the commercial antenna [32] at the Tx side are 0.75 dBi at 3 GHz, 3.25 dBi at 10 GHz and 6 dBi at 28 GHz. The gains of the homemade antenna [33] at the Rx side are 1.25 dBi at 3 GHz, 2.8 dBi at 10 GHz and 4.8 dBi at 28 GHz.

The close-in free space reference distance (CI) path loss model is utilized for fitting the PL with a single parameter n as [13], [36]

$$\text{PL}^{\text{CI}}(f, d)[\text{dB}] = \text{FSPL}(f, d_0) + 10 \cdot n\log_{10}(d/d_0) + X_\varsigma^{\text{CI}}$$
$$\text{for } d \geq d_0, \quad \text{where } d_0 = 1\,m \qquad (4)$$

where d_0 is the physically-based reference distance set as 1 m and $\text{FSPL}(f, d_0) = 10\log_{10}(\frac{4\pi d_0}{\lambda})^2$. d is the Tx-to-Rx distance, the linear slope n is well known as the path loss exponent (PLE), and X_ς^{CI} is the shadowing effect described by a Gaussian random variable with zero mean and standard

G. Zhang *et al.*: Modeling Multi-Frequency Characteristics for Classroom and Hall Scenarios at 2-4, 9-11 and 27-29 GHz Bands

IEEE *Access*

FIGURE 5. The example estimated PDASs for Tx position 5 in the hall scenario at multiple frequency bands. (a) 27-29 GHz. (b) 9-11 GHz. (C) 2-4 GHz.

deviation ς. In our case, FSPL(f, 1 m) is 42.0 dB, 52.4 dB and 61.4 dB for 2-4, 9-11 and 27-29 GHz, respectively.

The floating-intercept (FI) path loss model for fitting the measured PL with two parameters, which has been widely used in the WINNER II model, the 3GPP SCM and the COST 2100 model, is established as [9]

$$\text{PL}^{\text{FI}}(d)[\text{dB}] = \alpha + 10 \cdot \beta \log_{10}(d) + X_\varsigma^{\text{FI}} \qquad (5)$$

where α and β denote the intercept and the slope obtained via least-square fitting, and X_ς^{FI} is the shadow fading considered as a Gaussian random variable with zero mean and standard deviation ς. Fig. 6 and Table 2 show the path loss fitting and the model fitting parameters by both CI and FI path loss models for classroom and hall scenarios at 2-4, 9-11, 27-29 GHz. It can be observed that the PLE at 27-29 GHz in the hall scenario is much larger than theoretical PLE ($n = 2$) in free space, which mismatches the results of the LoS scenarios in [9], [13]–[15]. We conjecture that it is because of the short-measured distance range (less than 10 m) and strong reflections contributed from the PEC materials of
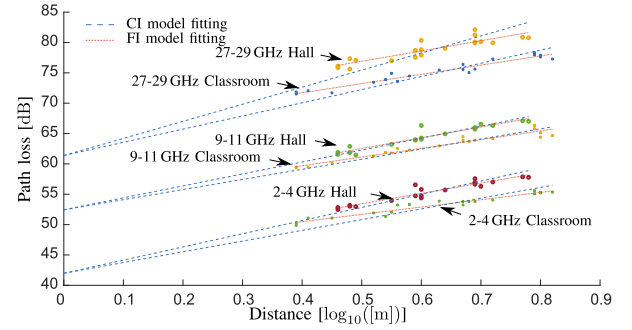
FIGURE 6. Path loss fitting for the path loss calculated based on the estimated data in classroom and hall scenarios at 2-4, 9-11, 27-29 GHz.
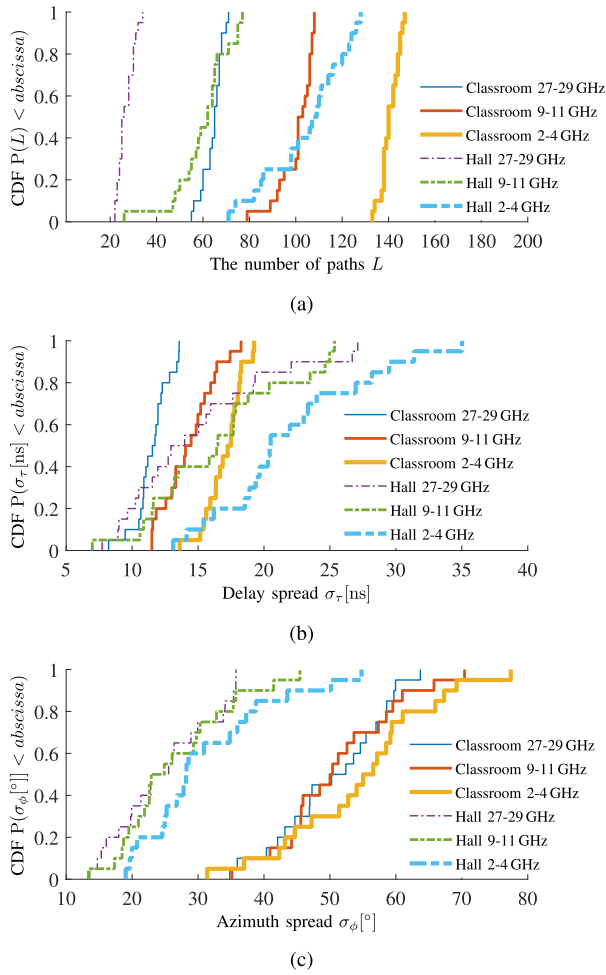
elevator and tubes in the hall scenario, which may lead to the overestimation of PLEs by the CI path loss model. Besides that, it is found that the PLEs are frequency independent in both classroom and hall scenarios, with similar conclusions for indoor scenarios found in [13]–[15]. In addition, it can also be found that both of the PLEs and β in the FI model in the classroom are smaller than those of the hall scenario at the same frequency. We speculate that it is because the Tx moves towards the east wall from Position 16 to Position 20 in the classroom scenario, there are strong reflections from the wall, which may lead to the underestimation of PLEs. Furthermore, the values of β in the FI model increase as the frequencies increase in the classroom scenario, with similar observation in [23]. However, similar values of β in the FI model at all bands are found in the hall scenario.

2) THE NUMBER OF PATHS L

The cumulative distribution functions (CDFs) of the number of paths L based on all the 20 Tx positions in both classroom and hall scenarios at multiple frequency bands are illustrated in Fig. 7(a), with statistical parameters (μ, σ) [2] in Table 2. It can be observed that the estimated L is smallest in the hall scenario at 27-29 GHz and largest in the classroom at 2-4 GHz. It can be found that the number of paths L increases as the frequency band decreases. Similar results were found in [9], [25] that the number of significant MPCs in the mm-wave band is much lower than that for below 6 GHz in similar scenarios. This is reasonable since mm-waves suffer more attenuation compared with lower frequency waves and less MPCs can be extracted within the same dynamic range, leading to a sparser channel at higher frequencies [25]. Besides that diffraction and diffuse scattering are more dominant at lower frequency bands [20], [23], [31], which are extracted as specular reflections in this paper, resulting in more specular paths at lower frequency bands. However, in the 3GPP model [39], the number of paths and the number of clusters are defined as the same for different frequency bands, which is inconsistent with the results found in the current work as well as the referred works. Furthermore, the number of paths L in the classroom is larger than that in the hall at the same frequency bands. It is reasonable as the dimension of the

---

[2] μ and σ represent mean value and variance, respectively.

IEEE *Access*

G. Zhang *et al.*: Modeling Multi-Frequency Characteristics for Classroom and Hall Scenarios at 2-4, 9-11 and 27-29 GHz Bands

(a)

(b)

(c)

FIGURE 7. Empirical CDFs of composite parameters for the classroom and hall scenarios at 2-4, 9-11 and 27-29 GHz frequency bands. (a) The number of paths *L*. (b) Delay spread σ_τ. (c) Azimuth spread σ_ϕ.

classroom is much smaller than the hall and more objects exist in the classroom, leading to more MPCs in the classroom.

3) COMPOSITE DELAY SPREAD σ_τ AND AZIMUTH SPREAD σ_ϕ

The RMS delay spread and azimuth spread are the parameters for characterizing the delay and azimuth dispersion of the channel. The RMS delay spread σ_τ is calculated as [37], [38]

$$\sigma_\tau = \sqrt{\overline{\tau^2} - \overline{\tau}^2} \qquad (6)$$

with

$$\overline{\tau^2} = \frac{\sum_{\ell=1}^{L} |\alpha_\ell|^2 \cdot \tau_\ell^2}{\sum_{\ell=1}^{L} |\alpha_\ell|^2}, \quad \overline{\tau} = \frac{\sum_{\ell=1}^{L} |\alpha_\ell|^2 \cdot \tau_\ell}{\sum_{\ell=1}^{L} |\alpha_\ell|^2} \qquad (7)$$

The RMS azimuth spread σ_ϕ is calculated as [39]

$$\sigma_\phi = \sqrt{-2\ln\left(\left|\frac{\sum_{\ell=1}^{L} \exp(j\phi_\ell) \cdot |\alpha_\ell|^2}{\sum_{\ell=1}^{L} |\alpha_\ell|^2}\right|\right)} \qquad (8)$$
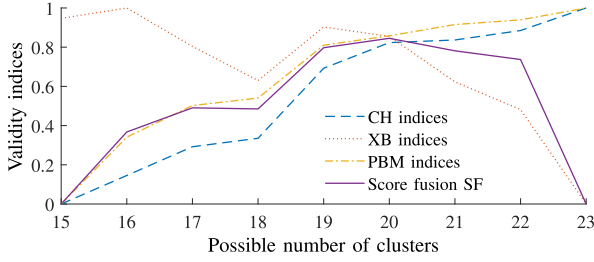
Fig. 7(b) and Fig. 7(c) illustrate the CDFs of σ_τ and σ_ϕ for the classroom and hall scenarios at all frequency bands,

with statistical parameters (μ, σ) in Table 2. It can be seen that the mean values of RMS delay spreads are 11.53 ns and 14.89 ns for the classroom scenario and hall scenario at 28 GHz, respectively, which are similar with the mean RMS delay spreads 12 ns for open office LoS scenario and smaller than 37 ns for shopping mall LoS scenario [40]. It can also be observed that the delay spreads increase as frequencies decrease in both classroom and hall scenarios. Similar to results reported in [13] when comparing RMS delay spreads of 28 and 73 GHz for indoor office LoS scenario. Furthermore, the mean values of RMS azimuth spreads are 50.30° and 24.79° for the classroom scenario and hall scenario at 28 GHz, respectively, which are larger than the mean azimuth spreads 19.6° at 28 GHz for the airport LoS scenario in [12] and also reported in the mmMAGIC project [34]. Besides that, the azimuth spreads are slightly larger at 2-4 GHz than those at higher frequency bands and mean azimuth spreads at 9-10 GHz and 27-29 GHz are similar in both classroom and hall scenario. Similar observation can be found in [12] that mean azimuth spreads are also similar at 15 and 28 GHz and larger than that at 60 GHz in airport LoS scenario. We conjecture that larger delay spreads and azimuth spreads at lower frequency bands are caused by the fact that more MPCs and more reflection orders exist at lower frequency bands, resulting in larger delay spreads and azimuth spread at lower frequency bands. Particularly, the azimuth spreads are similar at 9-11 and 27-29 GHz, due to the fact that the dominant reflections are mainly from similar azimuth angles at higher frequency bands. Furthermore, it can also be observed from Fig. 7(b) that in most cases, the delay spreads in the hall scenario are larger than that observed in the classroom scenario at the same frequencies. We postulate that the larger dimension of the hall leads to the MPCs with larger relative delays. While, in some cases, the delay spreads in the hall are smaller than that of the classroom, possibly due to that the pillars or tubes in the hall cause dominant paths leading to the whole spread being compressed. Moreover, it can also be observed from Fig. 7(c) that the azimuth spreads in the classroom are larger than that in the hall at all frequencies. It is probably due to the fact that the larger dimension of the hall and the reflections in the hall are mainly contributed by the pillar and tubes nearby, resulting in the compressed azimuth spread.

IV. CLUSTER CHARACTERISTICS
A. CLUSTER IDENTIFICATION

There exist several methods, e.g. visual inspection [41], KPowerMeans [42], [43] and multipath component distance (MCD)-threshold principle [44] for grouping the MPCs. Visual inspection is not available in the case of multi-dimensions, i.e., considering the delay, azimuth, and elevation of the MPCs. The MCD-threshold principle requires prior assumptions of the optimum threshold, which is physically linked to the cluster size or distribution. For the automatic KPowerMeans method [28], the cluster validation

G. Zhang *et al.*: Modeling Multi-Frequency Characteristics for Classroom and Hall Scenarios at 2-4, 9-11 and 27-29 GHz Bands

IEEE Access·

FIGURE 8. The examples of the CVIs for the classroom scenario at position 5 in 27-29 GHz frequency band.

provides a trustworthy estimate of the optimum number of clusters, and the cluster pruning algorithm improves visibility. However, the automatic KPowerMeans method lacks the ability of the initialization for the number of clusters and centroids at different bands, which are difficult to obtain in advance. In [20], it is found that the identified clusters with similar delay and azimuth are basically contributed from similar physical objects in the same Tx position at multiple frequency bands. In this work, a novel cluster identification algorithm based on the automatic KPowerMeans method [28] is proposed to group the MPCs into clusters at multiple frequencies, considering both the consistency and difference at different bands. Besides that, the specular reflections are dominant at 27-29 GHz and the frequency dependence of specular reflections was not found to be significant [29], [30]. Thus we group the estimated MPCs at middle and low frequency bands based on the cluster results (e.g. the number of the clusters and centroids) from the same Tx position at the high frequency bands, which enables us to track the similarities at different bands with low complexity and better accuracy. Note that, we only focus on the angular information at the Rx UCA side in this work, i.e., AOA, without considering the angles-of-departure (AOD).

Specifically, the MPCs at 27-29 GHz are clustered based on the automatic KPowerMeans method [28] by setting a range $[K_{min}, K_{max}]$ for the expected number of clusters firstly. Then for each possible K, the KPowerMeans procedure is performed to assign a cluster index to each MPC, and the result is validated by the cluster validity indices (CVIs), such as Calinski Harabasz index, Xie and Beni index, Pakhira-Bandyopadhyay-Maulik index [45]–[48]. These CVIs indicate the cluster's compactness, separation, and exclusiveness. The optimum number of clusters K_{opt} is determined according to the score fusion SF [47], [49] calculated as the geometrical mean of all the CVIs. Fig. 8 illustrates the example for the range of the number of clusters in 27-29 GHz at position 5 in the classroom scenario. Then the cluster pruning algorithm is implemented by discarding the clusters with power lower than 0.1% of the total power for improved visualization, resulting in the final number of clusters K_{final} lower than K_{opt}.

For the 2-4 and 9-11 GHz bands, the MPCs are clustered using the proposed cluster identification algorithm, according to the identified clusters at 27-29 GHz. The proposed cluster
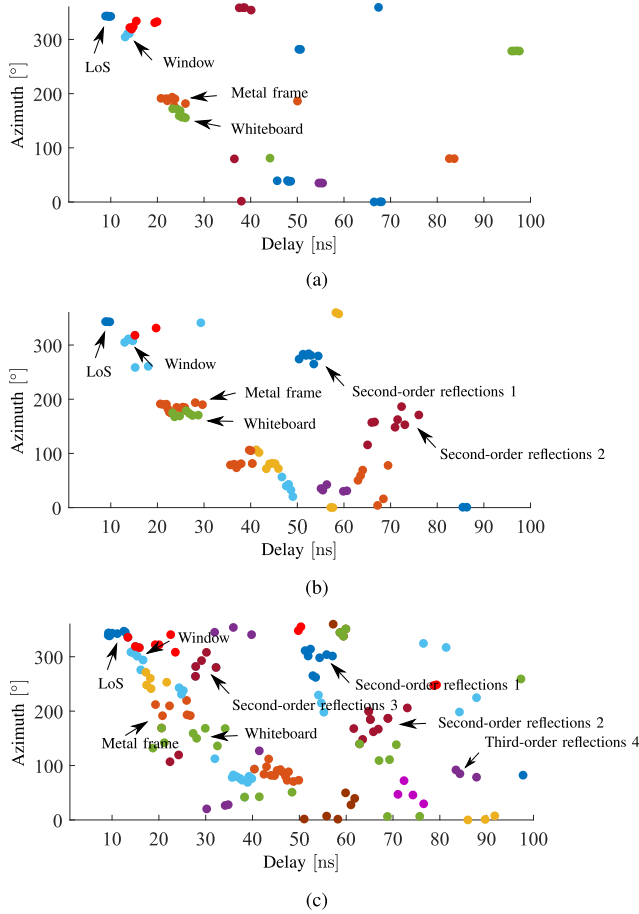

Algorithm 1 The Proposed Cluster Identification Algorithm Based on KPowerMeans Algorithm.

Input: MPC parameters α_ℓ, τ_ℓ, θ_ℓ at high and middle/low frequency.

Output: Middle/low frequency clustering results $\mathcal{L}_c^{(k')}$.

1: Cluster the MPCs at high frequency by the automatic KPowerMeans method [28], and obtain the cluster centroids $\mu_c^{(k)}$ and final clusters number K_{final},

2: Do for all number of clusters $K' = K_{final} + K'_{min}$ to $K_{final} + K'_{max}$, Do for all MCD distance threshold $\eta_{MCD} = \eta_{min}$ to η_{max}

   a. Assign MPCs at middle/low frequency to nearest cluster centroids $\mu_c^{(k)}$ and store the MCD distance

   b. Set the MCD distance threshold η_{MCD} and initialize $\mathcal{L}^{(k)}, \mathcal{L}^{(k')}$.

   c. Find the centroid index c_n with minimum MCD to the current MPC: $c_n = \arg \min_{c \in \mathcal{C}^{(k)}} \text{MCD}_{\ell, \mu_c^{(k)}}$

   d. for $\ell \in \mathcal{L}$ do

      if $\text{MCD}_{\ell, \mu_{c_n}^{(k)}} \leq \eta_{MCD}$ then

        $\mathcal{L}_{c_{previous}}^{(k)} \leftarrow \mathcal{L}_{c_{previous}}^{(k)} + \{\ell\}$

      else $\mathcal{L}_{c_{new}}^{(k')} \leftarrow \mathcal{L}_{c_{new}}^{(k')} + \{\ell\}$

      end if

    end for

   e. Recalculate the cluster centroids $\mu_{c_{previous}}^{(k')}$ from $\mathcal{L}_{c_{previous}}^{(k')}$, and cluster the $\mathcal{L}_{c_{new}}^{(k')}$ by the automatic KPowerMeans method [28], obtain the cluster centroids $\mu_{c_{new}}^{(k')}$

3: Find optimum number of clusters and optimum MCD distance threshold at middle/low frequency: $[K'_{opt}, \eta_{opt}] = \arg \max_{K', \eta_{MCD}} \text{SF}$

4: Prune optimum cluster set by removing the cluster power lower than 0.1% of total power

---

identification algorithm is elaborated in Algorithm 1. Firstly, assign the MPCs at middle and low frequency to the nearest cluster centroids $\mu_c^{(k)}$ obtained at high frequency and store the MCD distance. MCD distance [28] is used as the basic distance function between the MPC and nearest cluster centroid by the combination of delay and angular domain. A range of the MCD distance threshold $[\eta_{min}, \eta_{max}]$ is tested for choosing the optimum MCD distance threshold η_{opt} to separate the MPCs belonging to previous clusters $\mathcal{L}_{c_{previous}}^{(k')}$ obtained at the high frequency band and new clusters $\mathcal{L}_{c_{new}}^{(k')}$. At the middle and low frequency bands, the clusters found at the high frequency band are evaluated using the MCD distance for each of the MPCs, and the clusters only resulting in MCD distance larger than η_{MCD} are omitted. If the MCD distances are larger than η_{MCD}, these MPCs are stored for the new clusters $\mathcal{L}_{c_{new}}^{(k')}$ to be grouped using the automatic KPowerMeans method by adding the number of clusters range $[K'_{min}, K'_{max}]$. In this way, the KPowerMeans procedure only need be performed

IEEE *Access*

G. Zhang *et al.*: Modeling Multi-Frequency Characteristics for Classroom and Hall Scenarios at 2-4, 9-11 and 27-29 GHz Bands
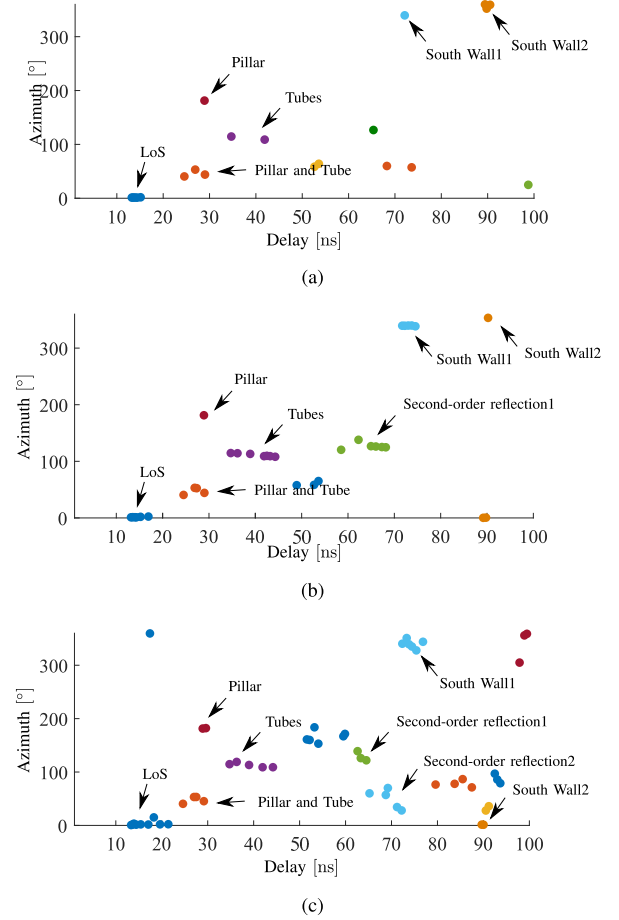
FIGURE 9. The examples of the cluster identification results for the classroom at position 5 in multiple frequency bands. (a) 27-29 GHz. (b) 9-11 GHz. (C) 2-4 GHz.
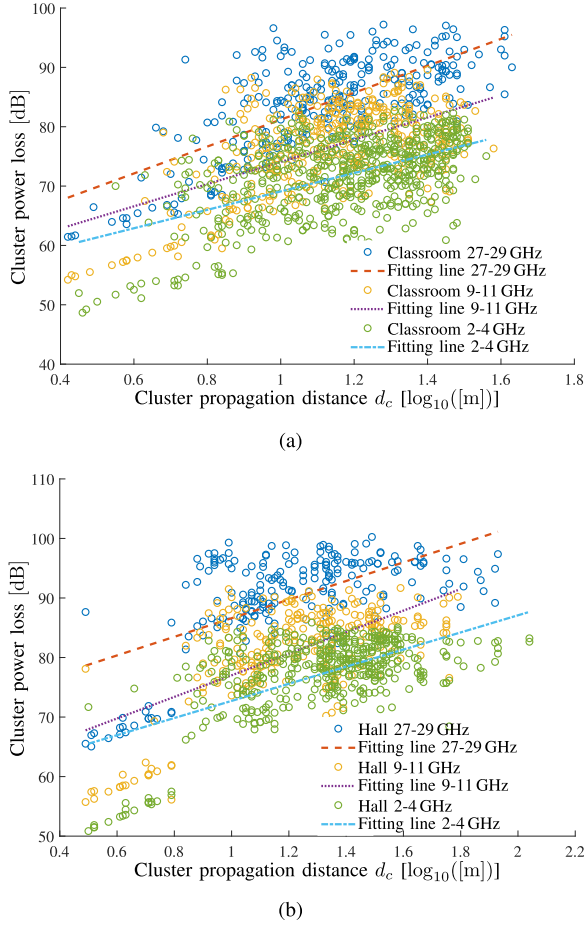

FIGURE 10. The examples of the cluster identification results for the hall at position 5 in multiple frequency bands. (a) 27-29 GHz. (b) 9-11 GHz. (C) 2-4 GHz.

for each possible K' in the range $[K'_{min}, K'_{max}]$ to iteratively initialize the cluster centroids and validate the results for the optimum number of clusters, which reduces the complexity of the clustering algorithm. The optimum number of clusters K'_{opt} and the optimum MCD distance threshold η_{opt} at middle and low frequency bands will be determined by the maximum value of the score fusion SF for all combinations of η_{MCD} and K'. Besides that, the cluster centroids of previous and new clusters are recalculated as

$$\mu_c = \frac{\sum_{\ell \in \mathcal{L}_c} |\alpha_\ell|^2 \cdot [\tau_\ell, \phi_\ell]^T}{\sum_{\ell \in \mathcal{L}_c} |\alpha_\ell|^2} \quad (9)$$

where T indicates transpose operation. Finally, we discard the clusters with power lower than 0.1% of the total power. Fig. 9 and Fig. 10 illustrate the examples of cluster identification results for the classroom and hall scenarios at position 5. In each figure, the dots with the same color represent the MPCs belonging to the same cluster. It can be observed from Fig. 9 that the clusters contributed from LoS paths, window, the metal frame of the whiteboard and the whiteboard in the classroom can be identified at all bands. Due to more diffuse scattering, diffraction and high order reflections at lower frequencies [20], the clusters of second-order reflection from

the windows and whiteboard are marked as "Second-order reflection 1" and "Second-order reflection 2", respectively, in both Fig. 9(b) and Fig. 9(c). Besides that, the clusters contributed by the second-order reflection from the window and third-order reflection from the southwest corner are marked as "Second-order reflection 3" and "Third-order reflection 4", respectively, in Fig. 9(c). Moreover, it can also be observed from Fig. 10 that the clusters from LoS, pillars, tubes and south wall in the hall can be identified at all bands. The clusters of second-order reflection from the tubes marked as "Second-order reflection 1" in both of Fig. 10(b) and Fig. 10(c), and the clusters contributed by the second-order reflection from the pillar marked as "Second-order reflection 2" in Fig. 10(c) are identified. Thus, the proposed novel cluster identification algorithm has the ability to cluster the MPCs contributed from similar objects at the same position in all bands reasonably.

B. CLUSTER LEVEL PARAMETERS
Based on the cluster identification results, the cluster-level parameters, i.e. the number of clusters, cluster delay spread, cluster azimuth spread and cluster power loss behavior are
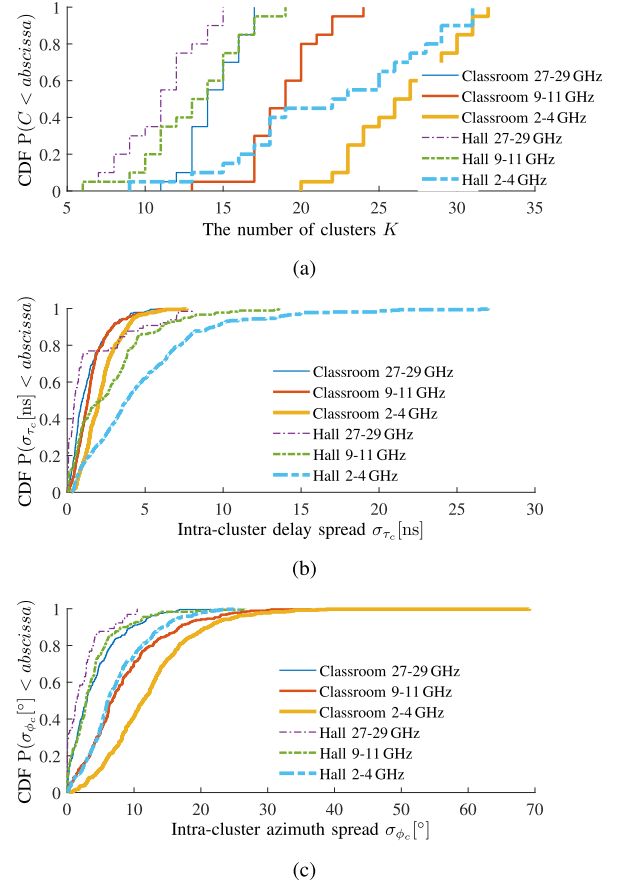
G. Zhang *et al.*: Modeling Multi-Frequency Characteristics for Classroom and Hall Scenarios at 2-4, 9-11 and 27-29 GHz Bands

IEEE *Access*

FIGURE 11. Cluster power loss behavior for classroom and hall scenarios at 2-4, 9-11 and 27-29 GHz frequency bands. (a) Classroom. (b) Hall.

FIGURE 12. The CDFs of cluster-level parameters for classroom and hall scenarios at 2-4, 9-11 and 27-29 GHz frequency bands. (a) The number of clusters K. (b) Intra-cluster delay spread σ_{τ_c}. (c) Intra-cluster azimuth spread σ_{ϕ_c}.

investigated. The statistics extracted for the cluster-level parameters of the proposed novel cluster identification algorithm and the automatic KPowerMeans method are detailed in Table 3.

1) CLUSTER POWER LOSS BEHAVIOR
To investigate the relationship between cluster power and delay, we analyze the cluster path loss behavior here. The cluster power loss was computed as the negative cluster total power and the propagation distance d_c was calculated based on the delay of the cluster centroid. Besides that, the standard deviation of cluster shadow fading was denoted as ς_c. The cluster power losses versus propagation distances in logarithmic scale fitted by the FI path loss model in (5) with linear regression lines for classroom and hall scenarios at 2-4, 9-11 and 27-29 GHz frequency bands are plotted in Fig. 11. It can be observed that the values of β increase as frequencies increase in the classroom, while it is different in the hall scenario, which is similar to the phenomenon of FI path loss β in Sect. III-C. In the classroom scenario, the higher frequency band waves have larger values of β, resulting in more rapid variations of cluster power versus distance.

2) THE NUMBER OF CLUSTERS K
Fig. 12(a) illustrates the CDFs of the number of clusters K for the classroom and hall scenarios at all bands. It can be observed that the number of clusters K increases as the frequency decreases in both the classroom and hall scenario, with similar results that the number of the clusters in mm-wave band is much lower than that for below 6 GHz in [9], [25]. It is reasonable that more diffuse scattering and diffractions exist at lower frequency band [20], resulting in more clusters. Besides that, at the same frequency the number of clusters K in the classroom is larger than that in the hall. We postulate that it is caused by the smaller dimension of the classroom and more objects in the classroom contribute more scattering points.

3) INTRA-CLUSTER DELAY SPREAD σ_{τ_c} AND AZIMUTH SPREAD σ_{ϕ_c}
Fig. 12(b) and Fig. 12(c) illustrate the CDFs of intra-cluster delay spread σ_{τ_c} and azimuth spread σ_{ϕ_c} for the classroom and hall scenarios at multiple frequency bands. It can be observed from Fig. 12(b) and Fig. 12(c) that both intra-cluster delay spreads and azimuth spreads increase as frequencies decrease. This is reasonable since more significant diffuse

IEEE Access

G. Zhang et al.: Modeling Multi-Frequency Characteristics for Classroom and Hall Scenarios at 2-4, 9-11 and 27-29 GHz Bands

TABLE 3. Statistics extracted for the cluster-level parameters.

		Parameters	Classroom	Hall
Automatic KPowerMeans	27-29 GHz	$PL_c (\alpha, \beta, \varsigma_c)$	(58.52, 2.27, 5.49)	(70.98, 1.56, 6.53)
		$K (\mu, \sigma)$	(14.40, 2.99)	(11, 6.63)
		σ_{τ_c} [ns] (μ, σ)	(1.33, 1.31)	(1.45, 4.55)
		σ_{ϕ_c} [°] (μ, σ)	(4.06, 15.34)	(2.34, 7.41)
	9-11 GHz	$PL_c (\alpha, \beta, \varsigma_c)$	(55.60, 1.83, 5.95)	(59.84, 1.68, 6.25)
		$K (\mu, \sigma)$	(17.95, 5.94)	(12.05, 5.21)
		σ_{τ_c} [ns] (μ, σ)	(1.72, 1.52)	(3.44, 10.69)
		σ_{ϕ_c} [°] (μ, σ)	(7.06, 22.35)	(4.53, 21.62)
	2-4 GHz	$PL_c (\alpha, \beta, \varsigma_c)$	(51.72, 1.59, 5.19)	(55.95, 1.51, 5.26)
		$K (\mu, \sigma)$	(21.95, 10.16)	(18.25, 8.51)
		σ_{τ_c} [ns] (μ, σ)	(2.66, 1.96)	(4.26, 7.94)
		σ_{ϕ_c} [°] (μ, σ)	(11.43, 33.06)	(9.16, 36.30)
Proposed Clustering Method	9-11 GHz	$PL_c (\alpha, \beta, \varsigma_c)$	(55.36, 1.87, 5.83)	(58.89, 1.81, 6.02)
		$K (\mu, \sigma)$	(18.90, 5.78)	(13.20, 10.27)
		σ_{τ_c} [ns] (μ, σ)	(1.54, 1.26)	(2.70, 6.67)
		σ_{ϕ_c} [°] (μ, σ)	(8.28, 40.36)	(3.79, 15.94)
	2-4 GHz	$PL_c (\alpha, \beta, \varsigma_c)$	(53.59, 1.55, 5.33)	(58.34, 1.44, 5.31)
		$K (\mu, \sigma)$	(28.15, 14.66)	(22.10, 39.67)
		σ_{τ_c} [ns] (μ, σ)	(2.08, 1.34)	(4.70, 14.90)
		σ_{ϕ_c} [°] (μ, σ)	(11.25, 37.02)	(7.25, 24.21)

scattering at lower frequency leads to more MPCs close to the strong reflections, which spread the delay and azimuth of the clusters. Moreover, it can also be observed from Fig. 12(b) that the intra-cluster delay spreads in the hall are larger than that observed in the classroom scenario at the same frequency bands. However, it can also be observed from Fig. 12(c) that the intra-cluster azimuth spreads in the hall are smaller than that observed in the classroom scenario at the same frequency bands. We conjecture it is because the clusters in the hall scenario are mainly from sparsely placed objects such as pillars, tubes and the sidewalls, which leads to larger cluster delay dispersion and smaller azimuth dispersion, as seen from the clusters contributed by the "Pillar and Tube" and "Tubes" in Fig. 10.

V. CONCLUSION

In this paper, wideband channel characteristics obtained in a classroom and a hall at 2-4, 9-11, 27-29 GHz were investigated. A high resolution parameter estimation (HRPE) algorithm was exploited to estimate the propagation parameters of the channel. A novel clustering identification algorithm based on the automatic KPowerMeans method was proposed to cluster the multipath components (MPCs) for 2-4, 9-11 and 27-29 GHz, where the consistency and dependency at different bands were well considered. The composite level and cluster level parameters were investigated. It can be observed that the PLE at 27-29 GHz in the hall scenario is much larger than theoretical PLE ($n = 2$) in free space, which mismatches the results of the LoS scenarios in [9], [13]–[15], mostly due to the short measured distance range (less than 10 m) and strong reflections contributed from the PEC materials of elevator and tubes in the hall scenario, resulting in the overestimation of PLEs by the CI path loss model. Besides that, it is found that the PLEs are frequency independent in both classroom and hall scenarios, with similar conclusions for indoor scenarios found in [13]–[15]. It is also found that the values of β in the FI path loss increase as the frequencies increase for the classroom scenario, but found to be frequency

independent for the hall. A similar phenomenon is observed with fitting parameter β of the cluster power loss in both scenarios. Furthermore, the number of paths, composite delay spread and azimuth spread, the number of clusters, and intra-cluster delay spread and azimuth spread increase as the frequency bands decrease in both scenarios. Similar results can be found in [9], [25] that the number of MPCs and the number of clusters in the mm-wave band is much lower than that for below 6 GHz in similar scenarios, known as channel sparsity. It is reasonable that scattering and diffraction are more dominant as the frequency decreased, as found in previously published works [20], [23], [31]. Moreover, the characteristics of the channel in classroom and hall scenarios at the same frequency bands have been compared for investigating the effect of the dimension and the objects in the scenarios on the channel. It is found that the number of paths and the number of clusters in the classroom are larger than that in the hall at the same frequencies, probably due to the fact that smaller dimension and more objects in the classroom lead to more reflection orders, resulting in more MPCs within the dynamic range. Additionally, composite delay spread and intra-cluster delay spread in the hall are basically larger than that observed in the classroom at all bands. However, the composite azimuth spread and intra-cluster azimuth spread in the classroom are larger than those in the hall at the same frequencies, mostly due to the fact that the objects in the hall can cause dominant paths. The established channel model can provide a valuable reference for evaluating the performance of 5G and beyond systems.

REFERENCES

[1] T. S. Rappaport, S. Sun, R. Mayzus, H. Zhao, Y. Azar, K. Wang, G. N. Wong, J. K. Schulz, M. Samimi, and F. Gutierrez, "Millimeter wave mobile communications for 5G cellular: It will work!" *IEEE Access*, vol. 1, pp. 335–349, 2013.

[2] M. Agiwal, A. Roy, and N. Saxena, "Next generation 5G wireless networks: A comprehensive survey," *IEEE Commun. Surveys Tuts.*, vol. 18, no. 3, pp. 1617–1655, 3rd Quart., 2016.

[3] J. G. Andrews, S. Buzzi, W. Choi, S. V. Hanly, A. Lozano, A. C. K. Soong, and J. C. Zhang, "What will 5G be?" *IEEE J. Sel. Areas Commun.*, vol. 32, no. 6, pp. 1065–1082, Jun. 2014.

[4] A. Osseiran, F. Boccardi, V. Braun, K. Kusume, P. Marsch, M. Maternia, O. Queseth, M. Schellmann, H. Schotten, H. Taoka, H. Tullberg, M. A. Uusitalo, B. Timus, and M. Fallgren, "Scenarios for 5G mobile and wireless communications: The vision of the METIS project," *IEEE Commun. Mag.*, vol. 52, no. 5, pp. 26–35, May 2014.

[5] M. Shafi, J. Zhang, H. Tataria, A. F. Molisch, S. Sun, T. S. Rappaport, F. Tufvesson, S. Wu, and K. Kitao, "Microwave vs. millimeter-wave propagation channels: Key differences and impact on 5G cellular systems," *IEEE Commun. Mag.*, vol. 56, no. 12, pp. 14–20, Dec. 2018.

[6] V. Nurmela, A. Karttunen, A. Roivainen, L. Raschkowski, V. Hovinen, J. Ylitalo, N. Omaki, K. Kusume, A. Hekkala, and R. Weiler, "Deliverable D1. 4 METIS channel models," Tech. Rep. ICT-317669-METIS/D1.4, 2015.

[7] Aalto University, BUPT, CMCC, Nokia, NTT DOCOMO, New York University, Ericsson, Qualcomm, Huawei, Samsung, Intel, University of Bristol, KT Corporation, University of Southern California, "5G channel model for bands up to 100 GHz," Tech. Rep., 2016. [Online]. Available: http://www.5gworkshops.com/5GCM.html

[8] *Study on Channel Model for Frequency Spectrum Above 6 GHz*, document 3GPP TR 38.900 version 14.2.0 Release 14, 2016.

[9] J. Ko, Y.-J. Cho, S. Hur, T. Kim, J. Park, A. F. Molisch, K. Haneda, M. Peter, D.-J. Park, and D.-H. Cho, "Millimeter-wave channel measurements and analysis for statistical spatial channel model in in-building and urban environments at 28 GHz," *IEEE Trans. Wireless Commun.*, vol. 16, no. 9, pp. 5853–5868, Sep. 2017.

[10] W. Roh, J.-Y. Seol, J. Park, B. Lee, J. Lee, Y. Kim, J. Cho, K. Cheun, and F. Aryanfar, "Millimeter-wave beamforming as an enabling technology for 5G cellular communications: Theoretical feasibility and prototype results," *IEEE Commun. Mag.*, vol. 52, no. 2, pp. 106–113, Feb. 2014.

[11] P. Zhang, J. Li, H. Wang, H. Wang, and W. Hong, "Indoor small-scale spatiotemporal propagation characteristics at multiple millimeter-wave bands," *IEEE Antennas Wireless Propag. Lett.*, vol. 17, no. 12, pp. 2250–2254, Dec. 2018.

[12] J. Vehmas, J. Jarvelainen, S. L. H. Nguyen, R. Naderpour, and K. Haneda, "Millimeter-wave channel characterization at helsinki airport in the 15, 28, and 60 GHz bands," in *Proc. IEEE 84th Veh. Technol. Conf. (VTC-Fall)*, Montreal, QC, Canada, Sep. 2016, pp. 1–5.

[13] G. R. Maccartney, T. S. Rappaport, S. Sun, and S. Deng, "Indoor office wideband millimeter-wave propagation measurements and channel models at 28 and 73 GHz for ultra-dense 5G wireless networks," *IEEE Access*, vol. 3, pp. 2388–2424, 2015.

[14] A. M. Al-Samman, T. A. Rahman, M. H. Azmi, M. N. Hindia, I. Khan, and E. Hanafi, "Statistical modelling and characterization of experimental mm-wave indoor channels for future 5G wireless communication networks," *PLoS ONE*, vol. 11, no. 9, Sep. 2016, Art. no. e0163034.

[15] A. M. Al-samman, T. Abd Rahman, and M. H. Azmi, "Indoor corridor wideband radio propagation measurements and channel models for 5G millimeter wave wireless communications at 19 GHz, 28 GHz, and 38 GHz bands," *Wireless Commun. Mobile Comput.*, vol. 2018, pp. 1–12, Mar. 2018.

[16] X. Wu, C.-X. Wang, J. Sun, J. Huang, R. Feng, Y. Yang, and X. Ge, "60-GHz millimeter-wave channel measurements and modeling for indoor office environments," *IEEE Trans. Antennas Propag.*, vol. 65, no. 4, pp. 1912–1924, Apr. 2017.

[17] J. Huang, C.-X. Wang, R. Feng, J. Sun, W. Zhang, and Y. Yang, "Multi-frequency mmWave massive MIMO channel measurements and characterization for 5G wireless communication systems," *IEEE J. Sel. Areas Commun.*, vol. 35, no. 7, pp. 1591–1605, Jul. 2017.

[18] K. Saito, P. Hanpinitsak, W. Fan, J.-I. Takada, and G. F. Pedersen, "Frequency characteristics of diffuse scattering in SHF band in indoor environments," in *Proc. URSI Asia–Pacific Radio Sci. Conf. (AP-RASC)*, New Delhi, India, Mar. 2019, p. 1.

[19] J. Medbo, N. Seifi, and H. Asplund, "Frequency dependency of measured highly resolved directional propagation channel characteristics," in *Proc. 22th Eur. Wireless Conf., Eur. Wireless*, Oulu, Finland, 2016, pp. 1–6.

[20] P. Hanpinitsak, K. Saito, W. Fan, J. Hejselbaek, J.-I. Takada, and G. F. Pedersen, "Frequency characteristics of geometry-based clusters in indoor Hall environment at SHF bands," *IEEE Access*, vol. 7, pp. 75420–75433, 2019.

[21] P. Hanpinitsak, K. Saito, W. Fan, J. Hejselbaek, J.-I. Takada, and G. F. Pedersen, "Cluster intensity and spread characteristics in classroom scenario at 10 and 28 GHz bands," in *Proc. 14th Eur. Conf. Antennas Propag. (EuCAP)*, Copenhagen, Denmark, Mar. 2020, pp. 1–3.

[22] P. Hanpinitsak, K. Saito, W. Fan, J. Hejselbaek, J. Takada, and G. F. Pedersen, "Multi-path Cluster characteristics in Indoor Environments at 28 GHz band," *IEICE Tech. Rep.*, vol. 119, no. 120, pp. 135–140, 2019.

[23] P. Hanpinitsak, K. Saito, W. Fan, J. Hejselbaek, J. Takada, and G. F. Pedersen, "Frequency characteristics of path loss and delay-angular profile of propagation channels in an indoor room environment in SHF bands," *IEICE Tech. Rep.*, vol. 116, no. 481, pp. 153–158, 2017.

[24] G. Zhang, K. Saito, W. Fan, X. Cai, P. Hanpinitsak, J.-I. Takada, and G. F. Pedersen, "Experimental characterization of millimeter-wave indoor propagation channels at 28 GHz," *IEEE Access*, vol. 6, pp. 76516–76526, 2018.

[25] A. Adhikary, E. Al Safadi, M. K. Samimi, R. Wang, G. Caire, T. S. Rappaport, and A. F. Molisch, "Joint spatial division and multiplexing for mm-wave channels," *IEEE J. Sel. Areas Commun.*, vol. 32, no. 6, pp. 1239–1255, Jun. 2014.

[26] X. Cai and W. Fan, "A complexity-efficient high resolution propagation parameter estimation algorithm for ultra-wideband large-scale uniform circular array," *IEEE Trans. Commun.*, vol. 67, no. 8, pp. 5862–5874, Aug. 2019.

[27] Y. Ji, W. Fan, and G. F. Pedersen, "Channel characterization for wideband large-scale antenna systems based on a low-complexity maximum likelihood estimator," *IEEE Trans. Wireless Commun.*, vol. 17, no. 9, pp. 6018–6028, Sep. 2018.

[28] N. Czink, P. Cera, J. Salo, E. Bonek, J.-P. Nuutinen, and J. Ylitalo, "A framework for automatic clustering of parametric MIMO channel data including path powers," in *Proc. IEEE Veh. Technol. Conf.*, Montreal, QC, Canada, Sep. 2006, pp. 1–5.

[29] D. Ferreira, I. Cuinas, R. F. S. Caldeirinha, and T. R. Fernandes, "A review on the electromagnetic characterisation of building materials at micro-and millimetre wave frequencies," in *Proc. 8th Eur. Conf. Antennas Propag. (EuCAP)*, The Hague, The Netherlands, Apr. 2014, pp. 145–149.

[30] G. Tesserault, N. Malhouroux, and P. Pajusco, "Determination of material characteristics for optimizing WLAN radio," in *Proc. Eur. Conf. Wireless Technol.*, Munich, Germany, Oct. 2007, pp. 225–228.

[31] W. Fan, I. Carton, J. Ø. Nielsen, K. Olesen, and G. F. Pedersen, "Measured wideband characteristics of indoor channels at centimetric and millimetric bands," *EURASIP J. Wireless Commun. Netw.*, vol. 2016, no. 1, p. 58, Dec. 2016.

[32] *A-INFO-SZ-2003000/P Datasheet*. [Online]. Available: http://www.ainfoinc.com/en

[33] S. S. Zhekov, A. Tatomirescu, and G. F. Pedersen, "Antenna for ultrawideband channel sounding," *IEEE Antennas Wireless Propag. Lett.*, vol. 16, pp. 692–695, 2017.

[34] Deliverable D2.2. Measurement Results and Final mmMAGIC Channel Models, "Millimetre-wave based mobile radio access network for fifth generation integrated communications, (mmMAGIC)," Tech. Rep., 2017.

[35] F. Zhang, W. Fan, and G. F. Pedersen, "Frequency-invariant uniform circular array for wideband mm-wave channel characterization," *IEEE Antennas Wireless Propag. Lett.*, vol. 16, pp. 641–644, 2017.

[36] M. K. Samimi, T. S. Rappaport, and G. R. MacCartney, "Probabilistic omnidirectional path loss models for millimeter-wave outdoor communications," *IEEE Wireless Commun. Lett.*, vol. 4, no. 4, pp. 357–360, Aug. 2015.

[37] X. Cai, J. Rodriguez-Pineiro, X. Yin, N. Wang, B. Ai, G. F. Pedersen, and A. P. Yuste, "An empirical air-to-ground channel model based on passive measurements in LTE," *IEEE Trans. Veh. Technol.*, vol. 68, no. 2, pp. 1140–1154, Feb. 2019.

[38] X. Cai, B. Peng, X. Yin, and A. P. Yuste, "Hough-transform-based cluster identification and modeling for V2V channels based on measurements," *IEEE Trans. Veh. Technol.*, vol. 67, no. 5, pp. 3838–3852, May 2018.

[39] *Study on Channel Model for Frequencies From 0.5 to 100 GHz*, document 3GPP TR 38.901 V16.1.0, Dec. 2019.

[40] L. Tian, J. Zhang, P. Tang, F. Huang, and Y. Zheng, "Delay characteristics for directional and omni-directional channel in indoor open office and shopping mall environments at 28 GHz," in *Proc. IEEE 27th Annu. Int. Symp. Pers., Indoor, Mobile Radio Commun. (PIMRC)*, Valencia, Spain, Sep. 2016, pp. 1–4.

[41] L. Vuokko, P. Vainikainen, and J. Takada, "Clusterization of measured direction-of-arrival data in an urban macrocellular environment," in *Proc. 14th IEEE Proc. Pers., Indoor Mobile Radio Commun. (PIMRC)*, Beijing, China, Sep. 2003, pp. 1222–1226.

[42] N. Czink, R. Tian, S. Wyne, F. Tufvesson, J.-P. Nuutinen, J. Ylitalo, E. Bonek, and A. F. Molisch, "Tracking time-variant cluster parameters in MIMO channel measurements," in *Proc. 2nd Int. Conf. Commun. Netw. China*, China, Shanghai, Aug. 2007, pp. 1147–1151.

[43] T. Hastie, R. Tibshirani, and J. Friedman, *The Elements of Statistical Learning: Data Mining, Inference, and Prediction* (Springer Series in Statistics), 2nd ed. Springer, 2009.

[44] C. Gustafson, K. Haneda, S. Wyne, and F. Tufvesson, "On mm-wave multipath clustering and channel modeling," *IEEE Trans. Antennas Propag.*, vol. 62, no. 3, pp. 1445–1455, Mar. 2014.

[45] S. Cheng, M.-T. Martinez-Ingles, D. P. Gaillot, J.-M. Molina-Garcia-Pardo, M. Lienard, and P. Degauque, "Performance of a novel automatic identification algorithm for the clustering of radio channel parameters," *IEEE Access*, vol. 3, pp. 2252–2259, 2015.

[46] U. Maulik and S. Bandyopadhyay, "Performance evaluation of some clustering algorithms and validity indices," *IEEE Trans. Pattern Anal. Mach. Intell.*, vol. 24, no. 12, pp. 1650–1654, Dec. 2002.

[47] K. Krzysztof and P. Hurley, "Estimation of the number of clusters using multiple clustering validity indices," in *Proc. Int. Workshop Multiple Classifier Systems*. Berlin, Germany: Springer, 2010, pp. 114–123.

[48] M. K. Pakhira, S. Bandyopadhyay, and U. Maulik, ''Validity index for crisp and fuzzy clusters,'' *Pattern Recognit.*, vol. 37, no. 3, pp. 487–501, Mar. 2004.

[49] X. Cai, G. Zhang, C. Zhang, W. Fan, J. Li, and G. F. Pedersen, ''Dynamic channel modeling for indoor millimeter-wave propagation channels based on measurements,'' *IEEE Trans. Commun.*, vol. 68, no. 9, pp. 5878–5891, Sep. 2020.

KENTARO SAITO (Member, IEEE) was born in Kanagawa, Japan, in 1977. He received the B.S. and Ph.D. degrees from the University of Tokyo, Japan, in 2002 and 2008, respectively. He joined NTT DOCOMO, Kanagawa, Japan, in 2002. Since 2002, he has been engaged in the research and development of mobile communication systems and radio propagation. He joined the Tokyo Institute of Technology, Japan, in 2015. Since 2015, he has been engaged in the research on radio propagation for mobile communication systems. Dr. Saito is a member of the IEICE.

GUOJIN ZHANG received the bachelor's degree in information engineering from the China University of Mining and Technology, China, in 2013, and the master's degree from the China University of Petroleum (East China), China, in 2016. She is currently pursuing the Ph.D. degree with the Antennas, Propagation and Millimeter-Wave Systems (APMS) Section, Aalborg University, Denmark. From July 2016 to January 2018, she was with Ericsson Communications, China, as a Network Engineer. The focus of her work is on channel parameter estimation and radio propagation channel modeling in millimeter wave frequency bands.

JESPER ØDUM NIELSEN received the master's degree in electronics engineering and the Ph.D. degree from Aalborg University, Denmark, in 1994 and 1997, respectively. He is currently employed at the Department of Electronic Systems, Aalborg University, Denmark, in the Antennas, Propagation and Millimeter-wave Systems section. His main areas of interests are experimental investigation of the mobile radio channel and the influence mobile device users have on the channel. Among other things, he has been involved in Massive MIMO and mm-wave channel sounding and modeling, as well as measurements using live LTE networks. In addition, he has been working with radio performance evaluation, including over the air testing of active wireless devices.

PANAWIT HANPINITSAK (Member, IEEE) was born in 1991. He received the B.E. degree (Hons.) in electronics and communications engineering from the Sirindhorn International Institute of Technology, Thammasat University, Pathumthani, Thailand, in 2013, and the M.E. degree in international development engineering, majoring in electrical/electronic engineering from the Tokyo Institute of Technology, Japan, in 2016, where he is currently pursuing the D.E. degree. His research interests include channel parameter estimation and beamforming algorithms, and radio propagation channel modeling at millimeter waves. He was a Guest Ph.D. Researcher with Aalborg University, Denmark, and the Ilmenau University of Technology, Germany, in 2016 and 2018, respectively. He received the Best Student Presentation Award at the IEICE Short Range Wireless (SRW) conference, in 2017. He is a Student Member of the IEICE.

XUESONG CAI received the B.S. and the Ph.D. degrees (Hons.) from Tongji University, Shanghai, China, in 2013 and 2018, respectively. In 2015, he conducted a three-month internship with Huawei Technologies, Shanghai, China. He was also a Visiting Scholar with Universidad Politécnica de Madrid, Madrid, Spain, in 2016. From 2018 to 2020, he was a Postdoctoral Research Fellow with the APMS section, Department of Electronic Sys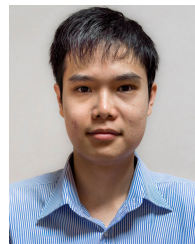tems, Aalborg University (AAU), Aalborg, Denmark. Since April 2020, he has been a Postdoctoral Fellow with the Wireless Communication Networks Section, Department of Electronic Systems, AAU, closely cooperating with Nokia Bell Labs. His research interests include propagation channel measurement, high-resolution parameter estimation, channel characterization, channel modeling, over-the-air testing, and UAV communications for 5G wireless communications. He was a recipient of the Chinese National Scholarship for Ph.D. Candidates and Excellent Student award in 2016, the Excellent Student award and the ''ZTE Fantastic Algorithm'' award in 2017, the Outstanding Doctorate Graduate awarded by the Shanghai Municipal Education Commission and ''ZTE Blue Sword-Future Leaders Plan'' in 2018, and the ''Seal of Excellence'' for the European Horizon 2020's Marie Skłodowska-Curie actions call in 2019.

JUN-ICHI TAKADA (Senior Member, IEEE) received the D.Eng. degree in electrical and electronic engineering from the Tokyo Institute of Technology (Tokyo Tech), in 1992. After serving as a Research Associate at Chiba University, from 1992 to 1994, and as an Associate Professor with Tokyo Tech, from 1994 to 2006. He has been a Professor at Tokyo Tech, since 2006. He is currently with the Department of Transdisciplinary Science and Engineering, School of Environment and Society, Tokyo Tech. From 2003 to 2007, he was also a Researcher with the National Institute of Information and Communication Technology, Japan. His current research interests include radio-wave propagation and channel modeling for mobile and short range wireless systems, applied measurement using radio wave, and ICT applications for international development. He is a fellow of the Information and Communication Engineering (IEICE), Japan, and a member of the Japan Society for International Development.

G. Zhang *et al.*: Modeling Multi-Frequency Characteristics for Classroom and Hall Scenarios at 2-4, 9-11 and 27-29 GHz Bands

IEEE *Access*

GERT FRØLUND PEDERSEN (Senior Member, IEEE) was born in 1965. He received the B.Sc. and E.E. (Hons.) degrees in electrical engineering from the College of Technology in Dublin, Dublin Institute of Technology, Dublin, Ireland, in 1991, and the M.Sc.E.E. and Ph.D. degrees from Aalborg University, Aalborg, Denmark, in 1993 and 2003, respectively. Since 1993, he has been with Aalborg University, where he is currently a Full Professor heading the Antennas, Propagation, and Millimeter-wave Systems LAB with 25 researchers. He is also the Head of the Doctoral School on wireless communication with some 40 Ph.D. students enrolled. He has published more than 500 peer-reviewed articles, six books, 12 book chapters, and holds over 50 patents. He has also worked as a Consultant for developments of more than 100 antennas for mobile terminals including the first internal antenna for mobile phones in 1994 with lowest SAR, first internal triple-band antenna in 1998 with low SAR and high TRP and TIS, and lately various multiantenna systems rated as the most efficient on the market. He has worked most of the time with joint university and industry projects and have received more than 21 *M* in direct research funding. He is also the Project Leader of the RANGE project with a total budget of over 8 *M* investigating high performance centimeter/millimeter-wave antennas for 5G mobile phones. He has been one of the pioneers in establishing over-the-air measurement systems. The measurement technique is now well established for mobile terminals with single antennas. He was chairing the various COST groups with liaison to 3GPP and CTIA for over-the-air test of MIMO terminals. He is also involved in MIMO OTA measurement. His research interests include radio communication for mobile terminals especially small antennas, diversity systems, propagation, and biological effects.
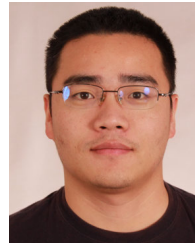
WEI FAN (Senior Member, IEEE) received the B.Eng. degree from the Harbin Institute of Technology, China, in 2009, the master's double degree (Hons.) from the Politecnico di Torino, Italy, and the Grenoble Institute of Technology, France, in 2011, and the Ph.D. degree from Aalborg University, Denmark, in 2014. From February 2011 to August 2011, he was with Intel Mobile Communications, Denmark, as a Research Intern. He conducted a three-month internship at Anite Telecoms oy (now Keysight Technologies), Finland, in 2014. He is currently an Associate Professor with the Antennas, Propagation and Millimeter-Wave Systems (APMS) Section, Aalborg University. His main research interests include over-the-air testing of multiple antenna systems, radio channel sounding, modeling and emulation, and antenna array signal processing.

● ● ●